NIH Public Access
Author Manuscript
Catheter Cardiovasc Interv. Author manuscript; available in PMC 2012 March 1.

Published in final edited form as:
Catheter Cardiovasc Interv. 2011 March 1; 77(4): 580–588. doi:10.1002/ccd.22787.

Therapeutic Ultrasound to Non-Invasively Create Intra-Cardiac Communications in an Intact Animal Model

Gabe E. Owens, M.D., Ph.D.
Department of Pediatrics, Division of Pediatric Cardiology University of Michigan, Ann Arbor, MI

Ryan M. Miller
Department of Electrical Engineering, University of Michigan, Ann Arbor, MI

Greg Ensing, M.D.
Department of Pediatrics, Division of Pediatric Cardiology, University of Michigan, Ann Arbor, MI

Kimberly Ives, D.V.M.
Department of Radiology, University of Michigan, Ann Arbor MI

David Gordon, M.D.
Department of Pathology, University of Michigan, Ann Arbor, MI

Achi Ludomirsky, M.D.
Department of Pediatric Cardiology, New York University, New York, NY

Zhen Xu, Ph.D.
Department of Biomedical Engineering, University of Michigan, Ann Arbor, MI

Abstract

Objective—To determine if pulsed cavitational ultrasound therapy (histotripsy) can accurately and safely generate ventricular septal defects (VSDs) through the intact chest of a neonatal animal, with the eventual goal of developing a non-invasive technique of creating intra-cardiac communications in patients with congenital heart disease.

Background—Histotripsy is an innovative ultrasonic technique that generates demarcated, mechanical tissue fractionation utilizing high intensity ultrasound pulses. Previous work has shown that histotripsy can create atrial septal defects in a beating heart in an open-chest canine model.

Methods—Nine neonatal pigs were treated with transcutaneous histotripsy targeting the ventricular septum. Ultrasound pulses of 5μs duration at a peak negative pressure of 13 MPa and a pulse repetition frequency of 1 kHz were generated by a 1 MHz focused transducer. The procedure was guided by real-time ultrasound imaging.

Results—VSDs were created in all pigs with diameters ranging from 2–6.5mm. Six pigs were euthanized within 2 hrs of treatment, while 3 were recovered and maintained for 2–3 days to evaluate lesion maturation and clinical side effects. There were only transient clinical effects and pathology revealed mild collateral damage around the VSD with no significant damage to other cardiac or extra-cardiac structures.

Conclusions—Histotripsy can accurately and safely generate VSDs through the intact chest in a neonatal animal model. These results suggest that with further advances, histotripsy can be a

Correspondence: Gabe Owens, 1500 East Medical Center Drive, Ann Arbor, MI 48109-5204 Phone: (734) 936-8997, Fax: (734) 232-3744, gabeo@med.umich.edu.

Disclosures None.

NIH-PA Author Manuscript
NIH-PA Author Manuscript
NIH-PA Author Manuscript

NIH-PA Author Manuscript

NIH-PA Author Manuscript

NIH-PA Author Manuscript

useful, non-invasive technique to create intra-cardiac communications, which currently require invasive catheter-based or surgical procedures, to clinically stabilize newborn infants with complex congenital heart disease.

Keywords

Pediatric Interventions; Ultrasonics; Echocardiography; Histotripsy

Introduction

Several forms of congenital heart disease benefit from the creation or enlargement of an intra-cardiac communication such as an atrial septal defect (ASD) to ensure appropriate delivery of oxygenated blood to essential organs (1–12). ASDs and less commonly ventricular septal defects (VSDs) are typically created in the fetus or neonate using cardiac catheterization or surgery with the associated risks of thrombo-embolic complications, cardiac perforation, and occasionally death.

Histotripsy is an innovative ultrasonic technique that generates demarcated, mechanical tissue fractionation utilizing high intensity focused ultrasound (HIFU) pulses, resulting in soft tissue breakdown. This technique utilizes controlled acoustic cavitation to produce mechanical tissue fractionation (13–15) rather than thermal necrosis used in other HIFU approaches (16–21). Cavitation bubbles are generated and maintained only at the focus leading to demarcated tissue fractionation and provide the ability to visually monitor therapy (22–27). Previous work has demonstrated that histotripsy can create clearly demarcated perforations in excised porcine atrial and ventricular tissues using appropriate acoustic parameters (28). In an open-chest canine model, histotripsy using an epicardial transducer position, accurately and efficiently generated ASDs without significant collateral damage or systemic clinical side effects (29).

The objective of this study was to determine if histotripsy could generate targeted intra-cardiac communications when positioned outside the body in an intact neonatal animal model. Safe creation of a targeted lesion in this manner, through multiple tissues layers including bone that may interfere with ultrasound propagation, should address the feasibility of this technique to create similar lesions in human neonates with congenital heart disease. Because vertical orientation of the heart in pigs limits ultrasound access to the atrial septum, the interventricular septum was targeted in this study.

Methods

The procedures described here have been reviewed and approved by the University Committee on Use and Care of Animals at the University of Michigan. Nine healthy neonatal (2–3 weeks) pigs weighing 3–5kg comparable, in size to the human neonate or infant, underwent percutaneous transthoracic histotripsy of the antero-apical muscular interventricular septum to avoid the conduction system.

The animals were pre-anesthetized with Telazol (6mg/kg, IM) and Xylazine (2.2mg/kg IM), intubated and maintained on Isoflurane (1–3%) inhalation anesthesia, and paralyzed with pancuronium (0.1mg/kg) for the duration of the procedure. Heparin (200units/kg) was administered prior to the procedure and every hour thereafter if necessary. During the histotripsy procedure, the pig was submerged neck deep in a semi-upright position (Fig. 1a) in degassed water, which ensures ultrasound propagation into the animal without forming cavitation in the propagation pathway. Each animal was monitored with pulse oximetry.

NIH-PA Author Manuscript

NIH-PA Author Manuscript

NIH-PA Author Manuscript

Histotripsy Apparatus

Ultrasound pulses for histotripsy treatment were generated by an external high power ultrasound therapy transducer. The transducer was placed in a degassed water filled cylinder covered by a thin plastic membrane that was acoustically transparent. The cylinder was then placed into the warm degassed water bath that contained the submerged pig. This ensured continued ultrasound coupling from transducer, to water, through plastic membrane, to water and then to the chest wall (Fig. 1a). An 8MHz imaging transducer (S8, SONOS 7500, Philips Healthcare, Andover, MA) was placed through the center hole of the therapy transducer (Fig. 1b) and coupled to the neonatal pig in the same manner.

The therapy transducer was designed in our laboratory and fabricated by Imasonic, S.A., Besançon, France. The circular transducer has a center frequency of 1 MHz, a geometric focal length of 90 mm, an outer diameter of 100 mm, and a 40 mm inner hole for housing an ultrasound imaging probe (Fig. 1b). Ultrasound pressure waveforms of this therapy transducer were previously measured in degassed water using a fiber optic probe hydrophone (30). The peak negative and positive pressures used in the following experiment were 16 MPa and 32 MPa, respectively. Taking into account the attenuation caused by the approximately 1.5 cm thick chest wall tissue in the pathway, the peak negative pressure reaching the ventricular septum was estimated to be 13 MPa, resulting in a mechanical index of 13 (31). The ultrasound pulses were 5 μs in duration (5 cycles at 1MHz) and separated by 1 ms (i.e., pulse repetition frequency = 1 kHz).

Histotripsy Treatment

Prior to the procedure, histotripsy pulses were applied to a water bath, producing a bright (hyperechoic) zone on a 2-dimensional ultrasound image. The front center of the hyperechoic zone was marked as the focal position (Fig. 2a). The bubble cloud generated in the water for identifying focal location is larger than that in the tissue or blood. During the treatment, the bubble zone visualized by ultrasound was measured to be approximately 2–4 mm wide.

An 8 or 12 MHz phased array imaging probe was used on the chest wall to identify a window which provided imaging of the anterior ventricular septum in the axial resolution without substantial overlying lung. The therapeutic transducer was then moved by a 3-axis positioning system (Parker Hannifin, Rohnert Park, CA, USA) to align the focus marker on the ventricular septum (Fig. 2b). The entire histotripsy procedure was guided by ultrasound imaging using an 8 MHz phased array probe inserted into the central hole of the therapy transducer.

To verify the targeting accuracy, a small number of pulses were applied to produce a bubble cloud on the RV portion on the muscular interventricular septum, usually anterior to the moderator band (Fig. 2c). Once the targeting was accomplished, respirations were held (in 1 minute intervals) and histotripsy treatment was applied to the ventricular septum. Ultrasound exposures were delivered in 1 minute intervals or until a hypoechoic (dark) channel was visualized through the ventricular septum. The area was interrogated with color Doppler to confirm the creation of a VSD.

Post-treatment Process

Within 2 hours after VSD creation, 6 of 9 animals were euthanized with a lethal dose of Pentobarbitol IV (100 mg/kg). In 3 animals, euthanasia was deferred for 2–3 days to evaluate sub-acute cellular changes related to histotripsy therapy and VSD creation. After euthanasia, the heart and lungs were extracted and fixed in a 10% formalin solution and

NIH-PA Author Manuscript

NIH-PA Author Manuscript

NIH-PA Author Manuscript

dissected after a week of fixation. The organs were first examined by gross evaluation and then processed with standard hematoxylin and eosin (H&E), phosphotungstic acid-hematoxylin (PTAH), and Gomori staining for pathological evaluation.

Results

Histotripsy applied extracorporeally propagated through multiple tissues layers including skin, bone, and portions of lung, and created a VSD in all 9 animals within 20 seconds to 4 minutes of therapy (Table I).

VSD creation was confirmed with 2-dimensional imaging, color flow Doppler (Fig. 3), and pathologic evaluation. The size of created VSDs was variable (2–6.5 mm). All animals tolerated the procedure. Minor complications including transient hypoxia and ventricular ectopy were self limited to the time during treatment. Seven animals received no intervention while 2 animals required epinephrine therapy for bradycardia. There were no major acute complications defined as pericardial effusion, sustained arrhythmia, or death. Two animals had mild unintended damage to the RV free wall due to its close proximity to the therapeutic focus. In the 3 animals, where euthanasia was deferred for 2–3 days post VSD creation, no changes in behavior, gait, appetite, vital signs, or other general characteristics were observed suggesting no global or neurologic effects from histotripsy treatment. VSD size also remained the same in these animals, although a surrounding rim of increased echogenicity was apparent, likely resulting from inflammation and/or edema (Fig. 4).

Evaluation of function prior to histotripsy therapy and immediately before euthanasia (either acute or after 2–3 days) revealed no overt differences in global ventricular contractility, although regional wall motion abnormalities could not be thoroughly evaluated in this acute study. Two dimensional and color flow Doppler analysis of the heart after treatment revealed no significant changes in valve function post procedure.

Gross Morphology

In all 9 neonatal pigs studied, the epicardial surfaces appeared intact (Fig. 5a–c). Seven animals had intact endocardial surfaces except for the created VSDs. In 2 animals where the bubble cloud did appear very close to the right ventricular anterior free wall, minor discoloration of the endocardial surface was visualized. No other unintended damage was visualized on gross examination.

Cardiac dissection of the 6 animals euthanized immediately post-procedure revealed demarcated damage in the ventricular septum. The VSD and surrounding hemorrhage indicated by dark colorization was observed on both sides of ventricular septum (Fig. 5d). In the 3 animals with delayed euthanasia, the lumen of the VSD was more demarcated with smooth walls and the flanking hemorrhage appeared less substantial (Fig. 5e).

Gross evaluation of the lungs revealed normal appearing lungs in 5 animals and very mild areas of congestion and focal hemorrhage in 4 comprising < 5% of lung tissue. No evidence of pulmonary embolus was found in the lungs on gross pathology in either the acute or sub-acute setting (Fig. 6a). The ribs and overlying tissue in the ultrasound pathway were also examined. No visible damage was observed.

Pathology

On H&E stained slides from animals immediately sacrificed, the central damage zone of the VSD contained acellular debris and platelet/fibrin deposits (Fig. 7a–b). The average zone of

NIH-PA Author Manuscript

NIH-PA Author Manuscript

NIH-PA Author Manuscript

necrosis in the center of the VSD was measured to be 3.7±0.7 mm (Table 1). VSDs from animals with delayed euthanasia had substantially less acellular debris (Fig. 7c) but were similar in size with a mean of 3.0±1.3 mm (Table 1).

Immediately outside the acellular zone in acutely euthanized animals was a rim of hemorrhage and structurally intact myocytes with a more eosinophilic hue and contracted nuclei in comparison to normal myocytes (Fig. 7b). These myocytes were likely affected by histotripsy. The width of hemorrhage (measured from the acellular zone border to distal portion of flanking injury on both sides of defect in multiple tissue slices and then averaged to provide a circumferential report of flanking injury) on the right ventricular side was 3.3±1.1 mm and on the left ventricular side 2.8±0.9 mm (Table I). Beyond this rim of damaged cells were normal appearing myocytes with no further discernable damage (Fig. 7b). In the animals allowed to survive 2–3 days, evaluation of the lesion revealed a clear lumen compared to the acutely sacrificed animals and the flanking region contained activated fibroblasts and occasional inflammatory cell invasion suggesting progression of an inflammatory remodeling process (Fig. 7c–d). The extent of flanking injury and/or inflammation was significantly less (1.3 mm vs. 3.3 mm on RV side and 1.2 mm vs. 2.8 mm on the LV side) comparing animals with delayed euthanasia to those with acute sacrifice (Table 1).

The areas of discoloration found in the right ventricular free wall in 2 animals described above corresponded to minor areas of contraction necrosis and hemorrhage suggesting the tissue was mildly affected by the histotripsy therapy. There were no areas of acellular debris or platelet/fibrin deposits. No other damage was noted in the heart on histological evaluation.

Histological evaluation of the lung revealed mostly normal appearing lung tissue with focal areas of congestion and hemorrhage (Fig. 6b). There was no evidence for thrombo-embolic events and no debris from tissue fractionation was seen as evaluated by Gomori trichrome and PTAH staining.

Discussion

Therapeutic creation of cardiac septal defects in necessary for the palliation of several forms of congenital heart disease (1–4,6,7,9,11,12) and is typically performed invasively with surgical or cardiac catheterization techniques (2,4,5). This study demonstrates feasibility of “non-invasive” creation of an intra-cardiac defect by percutaneous pulsed cavitational ultrasound or histotripsy. Nine VSDs were created in 9 intact neonatal pigs with minimal collateral damage or systemic side-effects.

The size of created VSDs was variable (2–6.5 mm), likely related to varying aberration of ultrasound energy from intervening bones and tissue, as well as motion and consistency of the targeted ventricular septum. However, no correlations could be definitively made between amount of overlying tissue (range 14–17 mm) or septal motion (range 2.6–5 mm) on VSD size. Flanking injury, comparable to that seen in ASD creation in the open-chest canine model (29), was also observed and likely related to some of the same factors. These variables should be deemphasized with an unobstructed acoustic window, such as the subcostal approach in human neonates (or other non-human primates), targeting of the thinner and less mobile atrial septum, as well as with improved transducer design allowing for motion tracking, ECG gating, and improved targeting (by decreasing focal distance and improving imaging resolution).

The pathologic evaluation of the animals allowed to survive 2–3 days after treatment revealed persistence in the size of VSD and less flanking injury with evidence of cellular

NIH-PA Author Manuscript

NIH-PA Author Manuscript

NIH-PA Author Manuscript

remodeling (activated fibroblasts and inflammatory cell invasion), suggesting that some of the early flanking injury may be salvageable if not reversible. Further delineation of this inflammatory response, lesion maturation, and any systemic complications is currently under investigation in long-term studies.

No thrombo-embolic events were observed, consistent with prior demonstrations that particles created by histotripsy are largely < 6 μm (the size of a red blood cell) (32), a size unlikely to cause harm (33). Still, more robust evaluation of end-organ complications such as thrombo-embolic events are currently being investigated by utilizing transcranial Doppler during treatment and diffusion MRI to evaluate brain and other end-organs after therapy. Preliminary MRI data have revealed no evidence of cerebral lesions up to 1 month after defect creation.

Conclusions

These data in combination previous data demonstrating effective creation of ASDs in an open-chest dog model suggest that “non-invasive” creation of both atrial and ventricular septal defects via histotripsy is potentially feasible in the human neonate. Further investigation into potential side effects (embolic risk, maturation of lesions, and longer follow-up), improved transducer focusing and size optimization, and refinement of the approach are underway and necessary to develop the clinical potential of histotripsy for congenital heart disease and other applications.

Acknowledgments

The authors thank Dr. Timothy L. Hall and Yohan Kim for their help with construction of the therapy transducer driving system and positioning device.

Funding Sources This research has been funded by grants from the National Institutes of Health R01-HL077629 and The Hartwell Foundation.

References

1. Aiyagari RM, Rocchini AP, Remenapp RT, Graziano JN. Decompression of the left atrium during extracorporeal membrane oxygenation using a transseptal cannula incorporated into the circuit. Crit Care Med. 2006; 34(10):2603–6. [PubMed: 16915115]
2. Holzer RJ, Wood A, Chisolm JL, Hill SL, Phillips A, Galantowicz M, Cheatham JP. Atrial septal interventions in patients with hypoplastic left heart syndrome. Catheter Cardiovasc Interv. 2008; 72(5):696–704. [PubMed: 18942130]
3. Hurwitz RA, Girod DA. Percutaneous balloon atrial septostomy in infants with transposition of the great arteries. Am Heart J. 1976; 91(5):618–22. [PubMed: 1266719]
4. O'Connor TA, Downing GJ, Ewing LL, Gowdamarajan R. Echocardiographically guided balloon atrial septostomy during extracorporeal membrane oxygenation (ECMO). Pediatr Cardiol. 1993; 14(3):167–8. [PubMed: 8415220]
5. Rashkind WJ. The complications of balloon atrioseptostomy. J Pediatr Surg. 1970; 76:649–650.
6. Seib PM, Faulkner SC, Erickson CC, Van Devanter SH, Harrell JE, Fasules JW, Frazier EA, Morrow WR. Blade and balloon atrial septostomy for left heart decompression in patients with severe ventricular dysfunction on extracorporeal membrane oxygenation. Catheter Cardiovasc Interv. 1999; 46(2):179–86. [PubMed: 10348539]
7. Rashkind WJ, Miller WW. Creation of an atrial septal defect without thoracotomy. A palliative approach to complete transposition of the great arteries. JAMA. 1966; 196(11):991–2. [PubMed: 4160716]
8. Meadows J, Pigula F, Lock J, Marshall A. Transcatheter creation and enlargement of ventricular septal defects for relief of ventricular hypertension. J Thorac Cardiovasc Surg. 2007; 133(4):912–8. [PubMed: 17382625]

NIH-PA Author Manuscript

NIH-PA Author Manuscript

NIH-PA Author Manuscript

9. Vlahos AP, Lock JE, McElhinney DB, van der Velde ME. Hypoplastic left heart syndrome with intact or highly restrictive atrial septum: outcome after neonatal transcatheter atrial septostomy. Circulation. 2004; 109(19):2326–30. [PubMed: 15136496]
10. Vida VL, Bacha EA, Larrazabal A, Gauvreau K, Thiagaragan R, Fynn-Thompson F, Pigula FA, Mayer JE Jr. del Nido PJ, Tworetzky W, et al. Hypoplastic left heart syndrome with intact or highly restrictive atrial septum: surgical experience from a single center. Ann Thorac Surg. 2007; 84(2):581–5. [PubMed: 17643639]
11. Lenox CC, Zuberbuhler JR. Balloon septostomy in tricuspid atresia after infancy. Am J Cardiol. 1970; 25(6):723–6. [PubMed: 5420909]
12. Sato T, Onoki H, Kano I, Horiuchi T, Ishitoya T. Balloon atrial septostomy in an infant with tricuspid atresia. Tohoku J Exp Med. 1970; 101(3):281–8. [PubMed: 5455859]
13. Xu Z, Fowlkes JB, Rothman ED, Levin AM, Cain CA. Controlled ultrasound tissue erosion: the role of dynamic interaction between insonation and microbubble activity. Journal of the Acoustical Society of America. 2005; 117(1):424–435. [PubMed: 15704435]
14. Xu Z, Fowlkes JB, Cain CA. A new strategy to enhance cavitational tissue erosion by using a high intensity initiating sequence. IEEE Trans Ultrasonics Ferroelectrics Freq Control. 2006; 53(8): 1412–1424.
15. Kieran K, Hall TL, Parsons JE, Wolf JS, Fowlkes JB, Cain CA, Roberts WW. Refining histotripsy: defining the parameter space for the creation of nonthermal lesions with high intensity, pulsed focused ultrasound of the in vitro kidney. J Urol. 2007; 178(2):672–6. [PubMed: 17574617]
16. Hacker A, Kohrmann KU, Back W, Kraut O, Marlinghaus E, Alken P, Michel MS. Extracorporeal application of high-intensity focused ultrasound for prostatic tissue ablation. BJU Int. 2005; 96(1): 71–6. [PubMed: 15963124]
17. Kennedy JE, Wu F, ter Haar GR, Gleeson FV, Phillips RR, Middleton MR, Cranston D. High-intensity focused ultrasound for the treatment of liver tumours. Ultrasonics. 2004; 42(1–9):931–5. [PubMed: 15047409]
18. Wu F, Wang ZB, Chen WZ, Wang W, Gui Y, Zhang M, Zheng G, Zhou Y, Xu G, Li M, et al. Extracorporeal high intensity focused ultrasound ablation in the treatment of 1038 patients with solid carcinomas in China: an overview. Ultrason Sonochem. 2004; 11(3–4):149–54. [PubMed: 15081972]
19. Tempany CM, Stewart EA, McDannold N, Quade BJ, Jolesz FA, Hynynen K. MR imaging-guided focused ultrasound surgery of uterine leiomyomas: a feasibility study. Radiology. 2003; 226(3): 897–905. [PubMed: 12616023]
20. Schmidt B, Antz M, Ernst S, Ouyang F, Falk P, Chun JK, Kuck KH. Pulmonary vein isolation by high-intensity focused ultrasound: first-in-man study with a steerable balloon catheter. Heart Rhythm. 2007; 4(5):575–84. Epub 2007 Jan 17. [PubMed: 17467623]
21. Ninet J, Roques X, Seitelberger R, Deville C, Pomar JL, Robin J, Jegaden O, Wellens F, Wolner E, Vedrinne C, et al. Surgical ablation of atrial fibrillation with off-pump, epicardial, high-intensity focused ultrasound: results of a multicenter trial. J Thorac Cardiovasc Surg. 2005; 130(3):803–9. [PubMed: 16153932]
22. Xu Z, Hall TL, Fowlkes JB, Cain CA. Optical and acoustic monitoring of bubble cloud dynamics at a tissue-fluid interface in ultrasound tissue erosion. Journal of the Acoustical Society of America. 2007; 121(4):2421–2430. [PubMed: 17471753]
23. Xu Z, Raghavan M, Hall TL, Chang C-W, Mycek M-A, Fowlkes JB, Cain CA. High Speed Imaging of Bubble Clouds Generated in Pulsed Ultrasound Cavitational Therapy - Histotripsy. IEEE Trans Ultrasonics Ferroelectrics Freq Control. 2007; 54(10):2091–2101.
24. Xu Z, Hall TL, Fowlkes JB, Cain CA. Effects of acoustic parameters on bubble cloud dynamics in ultrasound tissue erosion (histotripsy). Journal of the Acoustical Society of America. 2007; 122(1): 229–236. [PubMed: 17614482]
25. Xu Z, Raghavan M, Hall TL, Mycek M-A, Fowlkes JB, Cain CA. Evolution of bubble clouds produced in pulsed cavitational ultrasound therapy - histotripsy. IEEE Trans Ultrason Ferroelectr Freq Control. 2008; 5:1122–1132. [PubMed: 18519220]

NIH-PA Author Manuscript

NIH-PA Author Manuscript

NIH-PA Author Manuscript

26. Atchley AA, Frizzell LA, Apfel RE, Holland CK, Madanshetty S, Roy RA. Thresholds for cavitation produced in water by pulsed ultrasound. Ultrasonics. 1988; 26(5):280–5. [PubMed: 3407017]
27. Fowlkes JB, Crum LA. Cavitation threshold measurements for micro-second length pulses of ultrasound. J. Acoust. Soc. Am. 1988; 83:2190–2201. [PubMed: 3411016]
28. Xu Z, Ludomirsky A, Eun LY, Hall TL, Tran BC, Fowlkes JB, Cain CA. Controlled ultrasound tissue erosion. IEEE Transaction on Ultrasonics, Ferroelectrics, and Frequency Control. 2004; 51(6):726–736.
29. Xu Z, Owens G, Gordon D, Cain C, Ludomirsky A. Noninvasive creation of an atrial septal defect by histotripsy in a canine model. Circulation. 2010; 121(6):742–9. [PubMed: 20124126]
30. Parsons JE, Cain CA, Fowlkes JB. Cost-effective assembly of a basic fiber-optic hydrophone for measurement of high-amplitude therapeutic ultrasound fields. Journal of the Acoustical Society of America. 2006; 119(3):1432–40. [PubMed: 16583887]
31. Duck, FA. Physical Properties of Tissue. Academic Press Inc.; 1990.
32. Xu Z, Fan Z, Hall TL, Winterroth F, Fowlkes JB, Cain CA. Size Measurement of Tissue Debris Particles Generated from Mechanical Tissue Fractionation by Pulsed Cavitational Ultrasound Therapy - Histotripsy. Ultrasound in Medicine & Biology. 2009; 35(2):245–255. [PubMed: 19027218]
33. Eskandari M. Cerebral embolic protection. Semin Vasc Surg. 2005; 18(2):95–100. [PubMed: 15986327]

NIH-PA Author Manuscript

NIH-PA Author Manuscript

NIH-PA Author Manuscript

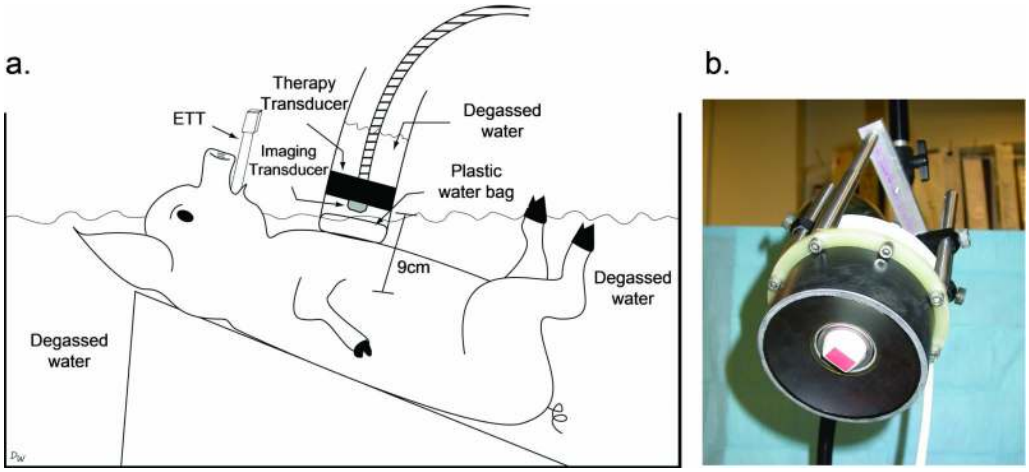

Figure 1.
Histotripsy setup. a) The neonatal pig is placed in a water bath. The therapy and imaging transducers are placed into a cylinder filled with degassed water and coupled to the pig's chest by a plastic membrane filled with water. b) Close-up view of 1MHz therapy transducer with an imaging transducer protruding through center opening.

Figure 2.
Generation of a cavitation bubble cloud. a) Prior to treatment, a cavitation bubble cloud is formed in degassed water to mark the focal point, seen by inserted arrow. b) The marked point is then positioned over the interventricular septum (IVS). c) Histotripsy is started and a hyperechoic bubble cloud is formed on the right ventricular (RV) side of the ventricular septum. LV (left ventricle)

NIH-PA Author Manuscript
NIH-PA Author Manuscript
NIH-PA Author Manuscript

NIH-PA Author Manuscript

NIH-PA Author Manuscript

NIH-PA Author Manuscript

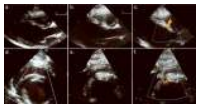

Figure 3.
Creation of VSDs by histotripsy. a) Image of the ventricular septum in long axis prior to treatment. b) After treatment a VSD is seen on 2 dimensional ultrasound imaging, and (c) shunting is seen across the ventricular septum with color flow Doppler. Another example of a created VSD is seen in short axis with images prior to treatment (a), post treatment (b) and with color flow Doppler (c).

NIH-PA Author Manuscript

NIH-PA Author Manuscript

NIH-PA Author Manuscript

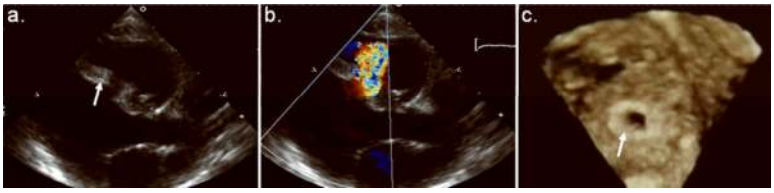

Figure 4.

VSD two days after histotripsy therapy. a–b) Parasternal long axis view of VSD two days after creation in 2D and with color flow Doppler. c) 3-dimensional representation of same VSD shown in a modified apical four chamber view showing persistence of the septal defect. Note the hyperechoic (bright) rim surrounding the defect marked by white arrows.

NIH-PA Author Manuscript

NIH-PA Author Manuscript

NIH-PA Author Manuscript

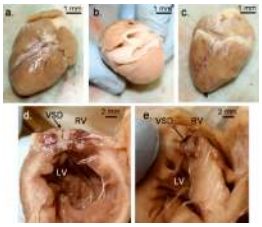

Figure 5.

Cardiac pathology after histotripsy treatment. Gross pathology of the heart revealed no damage to the epicardial surface on the anterior (a), basilar (b), or posterior regions (c). Dissection revealed demarcated damage across with ventricular septum with flanking zones of hemorrhage in immediately euthanized animals (d). e) Similar lesions were observed in animals with delayed euthanasia but with smoother borders and less apparent flanking hemorrhage and/or damage.

NIH-PA Author Manuscript

NIH-PA Author Manuscript

NIH-PA Author Manuscript

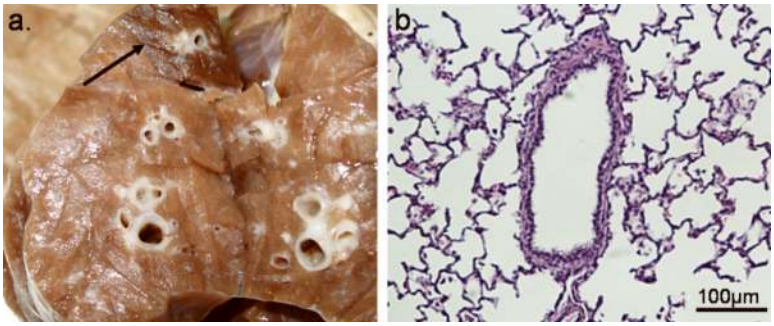

Figure 6.
Lung pathology. a) Gross evaluation of the lungs revealed mostly healthy appearing tissue with only focal areas of hemorrhage or congestion (arrow). On histological analysis (b) no microscopic evidence of thrombo-embolic events were visualized.

NIH-PA Author Manuscript
NIH-PA Author Manuscript
NIH-PA Author Manuscript

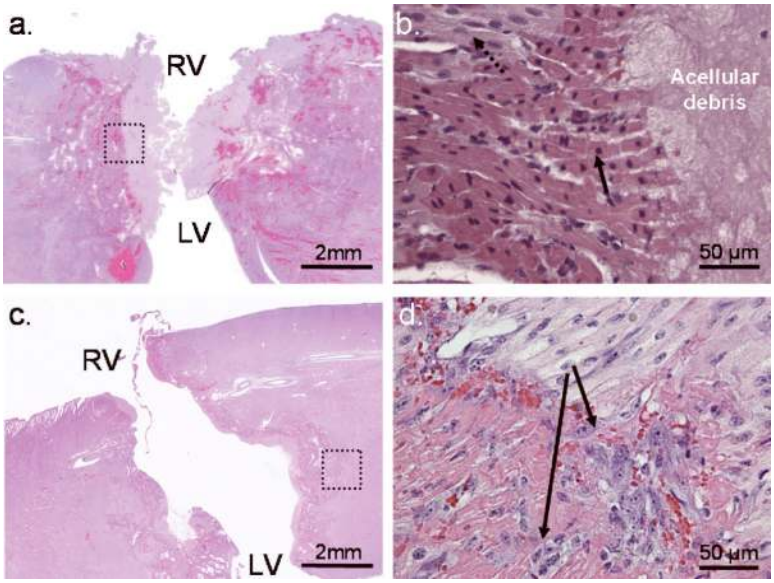

Figure 7.

Histology of ventricular septum. a) Histological analysis revealed a central area of acellular debris and necrosis and flanking areas of contraction necrosis with hemorrhage in immediately sacrificed animals. (b) High power imaging of this border reveals tight demarcation of necrosis and myocyte injury (solid arrow) with normal appearing myocytes in the top left of image (dashed arrow). c) In animals with delayed euthanasia, the VSD is more clearly demarcated without acellular debris and d) there is evidence of cellular remodeling with presence of activated fibroblasts (arrows).

NIH-PA Author Manuscript NIH-PA Author Manuscript NIH-PA Author Manuscript

Table 1

Summary of Histotripsy Treatments and Results

Case	Tx time (min)	Echo VSD size center (mm)	Path VSD size center (mm)	Flanking injury RV side (mm)	Flanking injury LV side (mm)	Complications
			Immediate euthanasia			
1	1.3	2.5	4	3.2	3.4	None
2	0.5	2.5	2.7	4.1	2.8	None
3	4	2	3.5	4.4	3.8	Bradycardia*
4	1.8	3.3	2.7	3.7	2.7	None
5	.33	4.2	4.4	3.3	2.7	Bradycardia*
6	3	6.5	5.2	1.2	1.1	None
Mean	**1.8**	**3.5**	**3.7**	**3.3**	**2.8**	
STD	**1.4**	**1.7**	**0.7**	**1.1**	**0.9**	
			Delayed euthanasia			
7	1.6	3.3	2.8	0.6	0.9	None
8	1.7	4	NA	1.9	1.1	None
9	2.4	2	3.1	1.3	1.6	None
Mean	**1.9**	**3.1**	**3.0**	**1.3** †	**1.2** †	
STD	**1.2**	**1.4**	**1.3**	**1.4**	**1.1**	

Echo VSD size center column represents measurements of the center of VSD from two-dimensional imaging. Path VSD size center is a measurement of the VSD on H&E slides measured at the center of the defect. Measurement for animal 8 is not available (NA) secondary to tissue processing. Flanking injury RV (right ventricle) and LV (left ventricle) side are measurements from H&E slides of flanking injury from the border of acellular debris/VSD to the outermost border of myocyte damage taken from both sides of the created defect at the RV and LV surfaces respectively, and then averaged. STD (standard deviation) Tx (therapy).

*both animals recovered after a single dose of epinephrine

†$p < 0.05$ by 2 tailed T-test when compared to immediate euthanasia group